TUDelft

Delft University of Technology

On-site drag analysis of drafting cyclists

Spoelstra, Alexander; Sciacchitano, Andrea; Scarano, Fulvio; Mahalingesh, Nikhil

Citation (APA)
Spoelstra, A., Sciacchitano, A., Scarano, F., & Mahalingesh, N. (2021). On-site drag analysis of drafting cyclists. *Journal of Wind Engineering and Industrial Aerodynamics*, *219*, Article 104797. https://doi.org/10.1016/j.jweia.2021.104797

Important note
To cite this publication, please use the final published version (if applicable).
Please check the document version above.

On-site drag analysis of drafting cyclists

Alexander Spoelstra [*], Andrea Sciacchitano, Fulvio Scarano, Nikhil Mahalingesh

Aerospace Engineering Department, Delft University of Technology, Kluyverweg 2, Delft, 2629 HT, the Netherlands

ABSTRACT

The aerodynamic drag of a trailing cyclists in a tandem formation is investigated at different lateral and longitudinal separations. A Ring of Fire (RoF) experiment is conducted at the Tom Dumoulin bike park of Sittard-Geleen in the Netherlands. The method is based on stereoscopic Particle Image Velocimetry (Stereo-PIV) measurements followed by invoking the conservation of momentum expressed in a control volume to evaluate the drag force of the cyclists. Three cyclists perform a series of individual tests as well as four different drafting tests, varying their order in the group. All tests were performed at a nominal riding speed of 45 km/h; the longitudinal displacement of the drafters varied between 0.32 m and 0.85 m and the lateral displacement varied between ±0.20 m among different runs. The results from the RoF measurements show the flow field interactions between the two drafting cyclists as well as the wake of the second cyclist. It is observed that the amount of drag reduction for the trailing rider is mainly caused by the change in inflow conditions. The drag reductions of the trailing cyclist are in the range from 27% to 66% depending on the longitudinal and lateral separation from the leading rider. The aerodynamic advantage of the drafting rider decreases with increasing lateral and longitudinal separation between riders, with the lateral separation found to be more relevant. Furthermore, based on the analysis of the individual wakes, the drag reductions found by the RoF, and the drag reduction measured by Barry et al. (2014), a model is introduced that predicts the aerodynamic gain of the trailing rider based on his or her position with respect to the leading rider. Validation of the model with data from literature shows that in the near wake the model prediction is in line with literature, with an overestimation of the drag reduction when the longitudinal distance is between 0.1 m and 0.3 m.

1. Introduction

In cycling jargon, drafting is a riding technique whereby a cyclist closely follows the preceding athlete, thereby substantially reducing the aerodynamic drag (Barry et al., 2015; Blocken et al., 2018; Broker et al., 1999). Already in 1953, Kawamura conducted wind tunnel measurements of two ¼ scaled cyclist models in racing position to quantify the drag benefits associated with drafting. The drag reduction experienced by the trailing cyclist was reported to decrease with the longitudinal separation, ranging from 54% at vanishing wheel gap and remaining as high as 40% at a 2 m separation (Kawamura, 1953). Wind tunnel tests with full-scale cyclists carried out by Zdravkovich (1996) in upright posture, with changes in the longitudinal and the lateral distance, led to the main conclusion that the drag reduction is rapidly lost by a lateral offset. For instance, a 20% drag increase with respect to the in-line configuration was observed already at an offset of 0.1 m.

Besides wind tunnel testing, drafting effects in cycling have been studied via Computational Fluid dynamics (CFD), offering full control on the shape, positions and postures of the riders (Blocken et al., 2013; Blocken et al., 2018; Defraeye et al., 2014; Íñiguez-De-La Torre and Íñiguez, 2009), at the cost however of some simplifications of the cyclist's geometry and motion, and of the flow behavior. Blocken et al. (2013) were the first to conduct numerical simulations of the tandem interactions for different cyclist postures. The simulations considered longitudinal separations up to 1 m, and no lateral offset. At the closest position, the numerical calculations returned the largest drag reduction for the trailing rider when both cyclists are in the upright position (27% drag reduction with respect to the isolated configuration). Instead, a drag reduction of only 14% was obtained in the time-trial position. Similarly to Zdravkovich (1996) and Kawamura (1953), the drag benefits showed a linear decay with increasing drafting distances, for all riders' postures. The discrepancy in drag reduction with respect to the previous experimental investigations of Kawamura (1953) and Zdravkovich (1996) may be ascribed to simplifications made in order to

---

* Corresponding author.
  E-mail address: A.M.C.M.G.Spoelstra@tudelft.nl (A. Spoelstra).

reduce the computational cost of the numerical simulations: the CFD model did not include the bicycles but only the riders. In particular, at 1 m separation and in upright position, a drag benefit of only 25% was reported, considerably lower than the value of 46% reported by Kawamura (1953). By investigating the flow field around the riders, Blocken et al. (2013) observed a reduction of the pressure ahead of the trailing cyclist and a slight pressure increase on the back surface (the "suction" region) of the trailing cyclist. This led to a reduced pressure deficit across the trailing cyclist, thus also to the drag reduction.

Most experimental data reported in the literature is obtained in wind tunnels or more directly during track tests. Barry et al. (2014) carried out wind tunnel experiments at full-scale for time-trial conditions and reported a maximum drag reduction of 49% for the trailing rider, supporting the findings of Zdravkovich (1996). At a separation of 0.7 m, 40% less drag was measured. Compared to Zdravkovich (1996), the decay rate for this aerodynamic benefit was 3 times smaller, leading again to a large discrepancy of approximately a factor two with respect to Zdravkovich's (1996) results. Whether such difference is to be ascribed to differences in posture, or experimental artifacts (e.g. high blockage ratio) remains not understood. Furthermore, Barry et al. (2014) confirmed that a lateral offset of the trailing cyclist goes rapidly to detriment to the drag reduction. Later experiments (Barry et al., 2016) have addressed the structure of the flow in the wake of a scaled cyclist model in a water tunnel by Particle Image Velocimetry (PIV). The authors identified the decreased streamwise momentum at the inflow experienced by the trailing cyclist as primary mechanism of drag reduction. As the longitudinal spacing was increased to 1.5 m, the energy recovery past the leading cyclist returned a situation close to that of an individual cyclist.

On-site experiments have been done with the coast-down technique (Kyle, 1979) and more recently using power meters (Broker et al., 1999; Edwards and Byrnes, 2007; Fitton et al., 2018). The results of Kyle (1979) showed a drag reduction of 38% for the trailing rider at a separation of 0.3 m (at a distance of 1.4 m the benefit reduced to 28%). The authors reported the limited control of the lateral offset among riders, as in cases where a lateral offset was observed, no drag reduction was actually found, qualitatively confirming the findings of Zdravkovich (1996) and Barry et al. (2014).

Broker et al. (1999) described an experiment with four cyclists featuring an aligned peloton, relevant to team time-trial racing. Experiments performed at an outdoor velodrome returned 29% less power delivered by the second rider than the leading cyclist. A reduction of 36% was reported for both third and fourth riders. Similar to the work of Kyle (1979), the limited control of spacing among riders led to some

inconsistencies in the data trends. Edwards and Byrnes (2007) report a mean drag reduction of 42% during track tests when drafting at 0.5 m longitudinal separation. In this case, the position was not monitored during experiments, contributing to experimental uncertainty.

The salient aspects from a selection of the above studies are summarized in Fig. 1, which indicates a drag reduction inversely proportional to both longitudinal separation and lateral offset. However, a striking dispersion of the drag values as well as its decay rate, especially with longitudinal separation, is remarked.

To the best of the authors' knowledge, all research up to now has dealt with discrete measurement points in the drafting region. Olds (1998) proposed a mathematical formula to take into in account the drag reduction of a drafting cyclist riding in-line with the leading cyclist. However, there has not yet been an attempt to model the drafting phenomenon mathematically in order to get a map that predicts the drafting effect at any given location. Moreover, it is clear that all of the current state-of-the art techniques for investigating cycling aerodynamics (wind tunnel, CFD and track measurements) have drawbacks when it comes to investigating the drafting effect in a realistic, but still controllable environment.

In recent years, a measurement concept has been introduced by the authors, named the Ring of Fire (RoF) (Spoelstra et al., 2019; Terra et al., 2017). The concept is based on large-scale stereoscopic Particle Image Velocimetry (stereo-PIV, Raffel et al., 2018) measurements in quiescent air where an object or a vehicle travels through it. The analysis of the momentum difference between the conditions prior to and after the passage poses the basis to estimate the aerodynamic drag. The measurement system was shown to provide the aerodynamic drag of an individual cyclist during sport action and returned a quantitative visualization of the flow field in the wake (Spoelstra et al., 2019). Thanks to the ability to measure the flow fields in the wake of both cyclists, as well as having a better monitoring of the posture and the relative distances between riders, the Ring of Fire system is in principle suitable for the investigation of the aerodynamics of a group of riders.

The aim of this work is to apply the RoF for drafting aerodynamics in cycling and provide insights into the flow field interactions between both cyclists. Furthermore, based on the wake development of an individual cyclist, a mathematical model is introduced to predict the drag of the trailing cyclist depending on his or her position relative to the leading cyclist.

2. Drag evaluation by momentum analysis

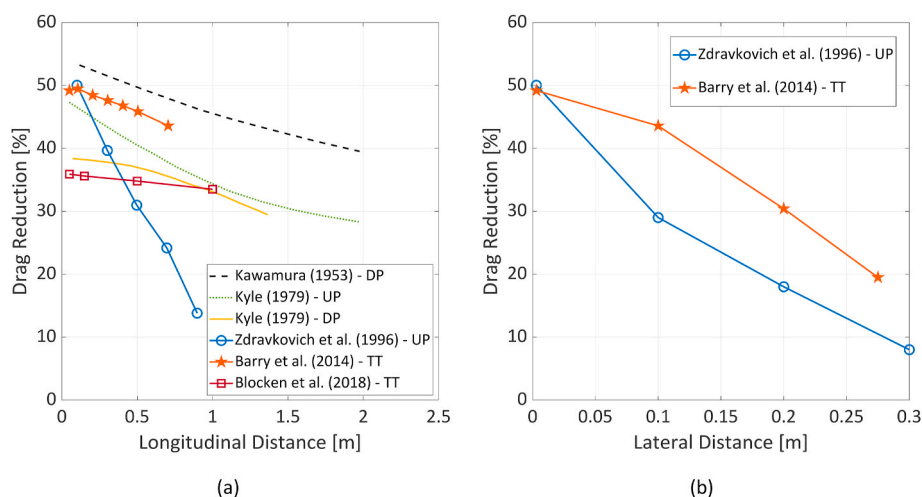The underlying principles for drag evaluation through the Ring of

Fig. 1. Overview of variations of trailing cyclist drag reduction by: (a) longitudinal offset; (b) lateral offset. Data covers different cycling postures: Time trial (TT), upright (UP) and dropped (DP). (Note: Effect of longitudinal distance taken at zero lateral offset. Effect of lateral distance taken at 0.1 m longitudinal separation).

Fire have been laid down in the works of Spoelstra et al. (2019) and Terra et al. (2017). The instantaneous drag force $D(t)$ is evaluated by invoking the conservation of momentum expressed in a control volume around a cyclist. The cyclists are assumed to move at constant speed u_C with respect to the laboratory frame of reference. In the case of an individual cyclist, the small and random air motions in the environment prior to the passage may be denoted as u_1 and the pressure as p_1. After the passage, the air is accelerated in the same direction as the cyclist, whose wake features a velocity field denoted as u_3 and a pressure field p_3. In case of an two cyclists, the velocity and pressure field in between both riders is denoted as u_2 and p_2, respectively. The drag of a group of cyclists can be determined similarly by including the whole group within the control volume (Fig. 2). When expressing velocity and momentum in the cyclists' frame of reference, the following expression returns the instantaneous drag of the group:

$$D(t) = \rho \underbrace{\iint_{S_1} (u_1 - u_C)^2 dS - \rho \iint_{S_3} (u_3 - u_C)^2 dS}_{Momentum\ term} + \underbrace{\iint_{S_1} p_1 dS - \iint_{S_3} p_3 dS}_{Pressure\ term} \quad (1)$$

where ρ is the air density. This expression is valid at the condition that the mass flow is conserved across surfaces S_1 and S_3. Also the drag of each individual cyclist can be calculated in the same way, namely by conservation of momentum across surfaces S_1 and S_2 for the leading cyclist, and surfaces S_2 and S_3 for the drafting one. In comparison to measurements for individual cyclists, where the trailing end of the control volume can be chosen far enough, such that the pressure term in equation (1) can be neglected, the pressure term needs to be considered between cyclists for an accurate drag evaluation (Terra et al., 2017).

3. Experimental set up and procedures

3.1. Facility and experimental conditions

Measurements are conducted at the Tom Dumoulin bike park of Sittard-Geleen in the Netherlands. The facility is built on a 6-ha area and hosts a total of 3.2 km track with paths that vary by surface type, differences in altitude, and challenging turns. Experiments are conducted on the 1.1 km, flat, oval outer lap. Three male professional cyclists from the DSM cycling team were recruited. A summary of their anthropometric characteristics and individual drag area (C_dA_0) and its confidence interval (CI) is reported in Table 1. The cyclists are named from A to C. The projected frontal area was determined from photographs taken from 5 m in front of the cyclist, with a reference area standing next to him. The frontal area was then determined as the average from multiple photographs at 4 different leg positions. As reported by Crouch et al. (2014) there are differences in frontal area of 2% between different leg

Table 1
Subjects' anthropometric characteristics and individual drag area (m²).

Subject	Height [m]	Mass [kg]	Projected frontal area [m²]	Drag area (C_dA_0) $\pm$ 95% CI [m²]	Number of passages
A	1.75	61	0.360	0.205 ± 0.012	7
B	1.85	70	0.337	0.182 ± 0.004	10
C	1.92	69	0.316	0.204 ± 0.005	11

positions. Therefore, the uncertainty on the projected frontal area is assumed to be 2%.

The cyclists were required to perform a series of individual tests as well as 4 different drafting tests, varying their order in the group. Fig. 3 shows one such passage of a drafting group (data not included here) through the Ring of Fire. All tests were performed at a nominal riding speed of 45 km/h; when drafting, the riders were asked to maintain a wheel-to-wheel spacing of 0.3 m and to stay in-line with the lead rider. In practice, the longitudinal displacement of the drafters varied between 0.32 m and 0.85 m and the lateral displacement varied between ± 0.20 m among different runs. The subjects were required to wear the same clothing and to use the same equipment during all testing sessions. In addition to the skin suit and helmet, the riders wore laser safety goggles for protection against the PIV laser light. For each configuration, the experiment was repeated 10 times. For all trials, the subjects started pedaling 300 m before the measurement region, accelerated to the prescribed velocity of 45 km/h and maintained such velocity up to about 100 m after the measurement region, where they ceased pedaling. The riders were also required to maintain a constant racing posture (time-trial posture) within and across all trials.

3.2. PIV system

The velocity distribution upstream and in the wake of the cyclists was obtained by large-scale stereoscopic-PIV. Neutrally buoyant helium-filled soap bubbles (HFSB) with an average diameter between 0.3 and 0.4 mm were used as flow tracers (Scarano et al., 2015), providing sufficient light scattering to visualize a field of view (FOV) of the order of 4 m². A tunnel of $8 \times 5 \times 3$ m³ in X, Y, and Z-direction (see Fig. 3) was used to confine the bubbles within the measurement volume. The tunnel had an open in- and outlet to allow the rider to transit and was equipped with optical access on one side for illumination purposes. The tracers were introduced in the measurement region by a rake with 200 nozzles positioned 1 m upstream of the measurement plane and aside the cyclists track. A Quantronix Darwin Duo Nd:YAG laser provided pulsed illumination (pulse energy of 2×25 mJ at 1 kHz rate). The laser beam was shaped into a 50 mm thick sheet by means of laser optics and light stops.
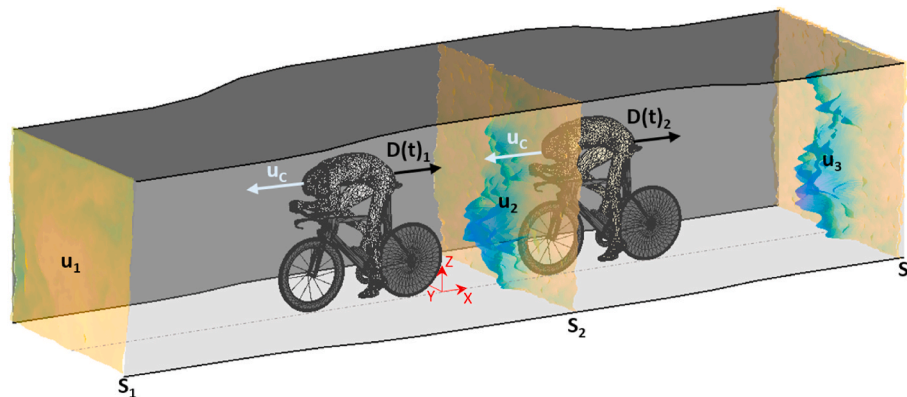
Fig. 2. Schematic view of the domain of interest, with two cyclists. S_1 and S_3 are the upstream and downstream sides of the domain. A color-coded surface illustrates the air velocity before, in between and after the passage of the group. (For interpretation of the references to color in this figure legend, the reader is referred to the Web version of this article.)
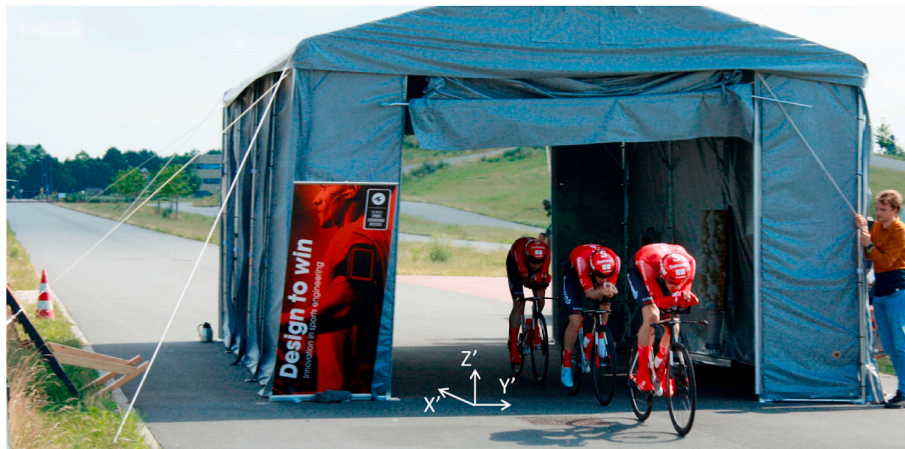
Fig. 3. Photograph of a three-cyclists group transiting across the Ring of Fire (Spoelstra et al., 2020b).

The field of view was imaged by two Photron Fast CAM SA1 cameras (CMOS, 1024 × 1024 pixels, 12 bits) equipped with 35 mm objectives at f/2.8. Images were acquired at 0.5 kHz and 1 kHz for the individual and drafting measurements, respectively. The cameras were placed 4 m upstream of the measurement plane with an angular separation of 95°, imaging a field of view of 1.8 × 1.8 m². The resulting magnification factor was 0.011 and the digital image resolution 0.57 px/mm. The tracers particles were held in the measurement domain by closing entrance and exit gates of the tunnel before the passage of the cyclist, accumulating for about 2 min. The velocity and position of the cyclists were determined from the stereo-PIV recordings. The resulting uncertainties are 0.1 m/s and 2 cm, respectively. A detailed sketch of the top view of the experimental setup is given in Fig. 4.

In this work, two right-hand coordinate systems are introduced; the system of reference that moves with the leading cyclist is denoted with (X,Y,Z) with the origin at the rearmost point of the rear wheel (Fig. 2). A stationary system of coordinate (X',Y',Z') is used to represent the positions along the track and the measurement location (Fig. 4). In both coordinate systems the Z-axis is the vertical axis, positive upwards.

3.3. Data reduction

The recorded images were processed with the LaVision DaVis 8.4 software by means of cross-correlation analysis. Following Spoelstra et al. (2020a), the final interrogation window size is chosen to be 24 × 24 pixels and the overlap factor is set to 75%. The evaluation of the cyclist drag via the control volume approach requires that mass conservation at the inflow and outflow of the domain is accurately satisfied, assuming there is no momentum transfer through the side faces of the domain. This assumption, however, is not possible in the current measurements as the velocity along the sides of the domain is not known. A way to mitigate the errors associated to approximate mass conservation is reducing the momentum analysis to the region where most deficit has occurred. This is done by means of a dedicated wake contouring

approach that is discussed in Spoelstra et al. (2020a) . Furthermore, the pressure field is reconstructed by solving the pressure Poisson equation (PPE) (van Oudheusden, 2013). Neumann boundary conditions are applied at the boundaries and the resulting pressure distribution is scaled with the measured quiescent air pressure as reference.

The ensemble-average drag area for the individual cyclists is computed for each cyclist. The final number of passages used for ensemble-averaging after discarding the faulty ones is presented in Table 1. For every passage of the cyclists, only the first 2.5 m in the wake are considered for drag calculation. On the basis of the evaluation of drag area from wake flow measurements at different distances from the cyclist, it is concluded that the windy conditions in the outdoor test facility cause the aerodynamic drag measurements beyond 2.5 m (0.2 s after the cyclist has passed) to become unreliable. Furthermore, the riders transited the laser sheet with no predefined crank-angle, meaning that the crank-angle at the laser sheet location varied from run to run.

The streamwise velocity in the (X,Y,Z) frame of reference is made dimensionless with the cyclist velocity u_C and reads as:

$$u_x^* = \frac{u_{wake} - u_C}{|u_C|} \tag{2}$$

With the above definition $u_x^* = 1$ occurs outside of the wake (no velocity deficit). When $u_x^* = 0$ the wake velocity deficit equals that of the cyclist (*dead air* region). Unless differently specified, u_x^* refers to the ensemble-average wake velocity. The drafting separation is defined as the distance between the rear wheel of the leading cyclist and the front wheel of the drafting one. The drag reduction coefficient *DR* for the trailing cyclist is defined as:

$$DR = \frac{C_dA_0 - C_dA_{draft}}{C_dA_0} \times 100 \tag{3}$$

and expresses the drag area reduction experienced by the trailing cyclist compared to riding alone. Accordingly we introduce the drag area C_dA_0
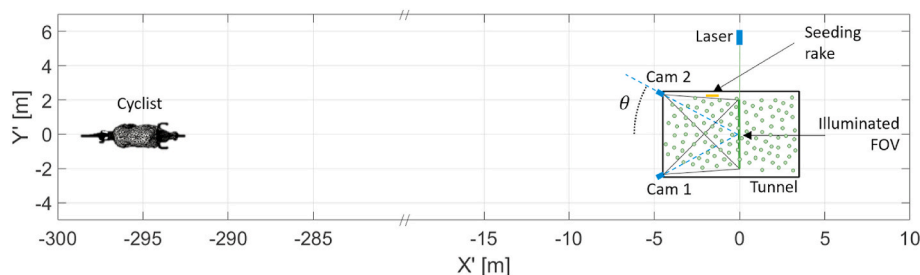

Fig. 4. Schematic view of the experimental setup.

of the rider alone and C_dA_{draft} for the drafting cyclist.

4. Results

In order to analyze the drafting effect in the tandem configuration, first the three single-rider tests are analyzed before the drafting scenarios are considered. In addition to the individual drag area of each of the cyclists, also the development of the time-average wake of an individual cyclist is evaluated. Next, the drafting configurations are studied. Firstly, three distinct runs are chosen for the investigation of the flow fields, after which the measured drag reductions are reported.

4.1. Effect of the human factor

On track measurements with real cyclists are affected by variations of the cyclists' speeds, positions, drafting distances, and environmental conditions, which all contribute to the measurement uncertainty. In wind tunnel measurements or CFD simulations these parameters are strictly controlled and any uncertainty arising from them is kept low. The drafting experiment with the Ring of Fire uses human subjects in a real world environment, which makes control of these parameters very hard. The impact of the human factor on the uncertainty of the measurement also gives a good indication on the uncertainty to be expected during racing performance.

An example of the effect of such a human factor is shown in Fig. 5, where cyclist A is shown to use different head postures in different passages. It was found that adopting a "head down" posture exposed more of the helmet tail to the freestream, while the "head up" posture tucked the helmet tail behind the head, shielding it from the freestream. This difference in head posture resulted in a maximum difference of 0.0158 m^2 in drag area for the two runs shown in Fig. 5, which translates to 7.7% of the mean drag area, thus explaining the higher statistical spread of C_dA_0 for cyclist A (Table 1).

Another parameter affected by the human factor was the drafting location. Despite the instruction given to the riders to maintain an aligned configuration at 0.3 m longitudinal distance, the analysis of the recorded images showed that there is a large variation in drafting distances between different runs from the same configuration as well as between different configurations. The average and standard deviation of drafting distances maintained by each cyclist while trailing another cyclist are obtained from 10 runs and are presented in Table 2.

On average, it is noticed that cyclist B performed best in maintaining a constant distance of 0.3 m from the leading rider, while cyclist A has twice the average longitudinal drafting distance. Also in terms of the lateral separation cyclist A is outperformed by the other cyclists. Thus

Table 2

Mean longitudinal and lateral separations for each cyclist in trailing position and the corresponding standard deviation obtained from 10 runs.

Configuration	$\overline{\Delta X}_{meas} \pm \sigma$ [cm]	$\overline{\Delta Y}_{meas} \pm \sigma$ [cm]
C – A	68 ± 8	6 ± 8
C – B	32 ± 4	2 ± 5
A – C	50 ± 7	5 ± 6
B – A	69 ± 10	7 ± 9

ranking the three subjects from skilled to less skilled in drafting, subject B is the most skilled and A the least.

4.2. Single cyclist

For each of the three cyclists, the planar cross sections (at X = 0.5 m) of the ensemble-average velocity and pressure coefficient in the wake are given in Fig. 6 and Fig. 8, respectively. In Fig. 6, a high deficit region is observed at Z < 0.5 m, which is ascribed to the aerodynamic resistance from the rear wheel and the drive train. Such deficit is more pronounced as one approaches the rear wheel. A second important area of deficit is observed between Z = 0.7 m and Z = 0.9 m, which corresponds to the vortices shed from the inner thigh and lower hip of the cyclist (Crouch et al., 2014). Finally, the region of deficit at Z = 1.2 m corresponds to the upper body and head of the cyclist.

A detailed comparison of the ensemble-average wake region contours ($u_x^* = 0.9$) for the three cyclists is illustrated in Fig. 7. The wake of cyclists B and C only differ in the upper part, consistent with their body size. Instead, the wake of cyclist A exhibits clear *appendices* indicating a wider position of the elbows/upper arms.

A comparison of the total pressure coefficient in the wake of the cyclists reveals that for all a low pressure is found in the lower half of the wake. Similar to the velocity fields, this is caused by the rear wheel and the drive train being closest to the measurement plane. For cyclist A, however, the low pressure is more spread out over the entire wake, which would indicate that the position of his upper body is less streamlined and thus acting more like a bluff body as compared to the other two cyclists. The similarity between velocity and total pressure here can be explained by the fact that the static pressure only accounts for roughly 10% of the total pressure and thus the total pressure is dominated by the dynamic pressure.

The spatial evolution of the velocity field along the wake of cyclist C is shown in Fig. 9. A deficit of 20% (10%) extends up to 6 m (beyond 10 m), indicating that drag benefits can be obtained from drafting even several meters behind the preceding cyclist. However, the high deficit

(a)   (b)
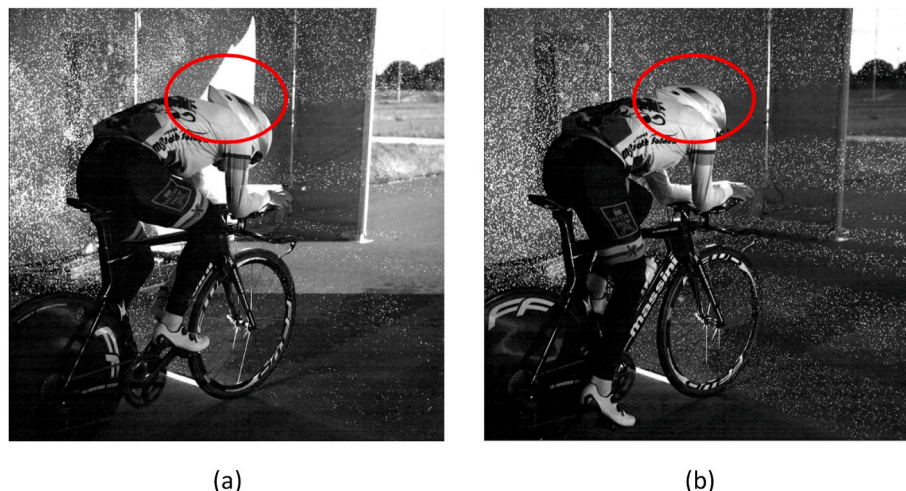
Fig. 5. Variations of head posture between different cyclist passages. (a) Head down position vs. (b) head up position.
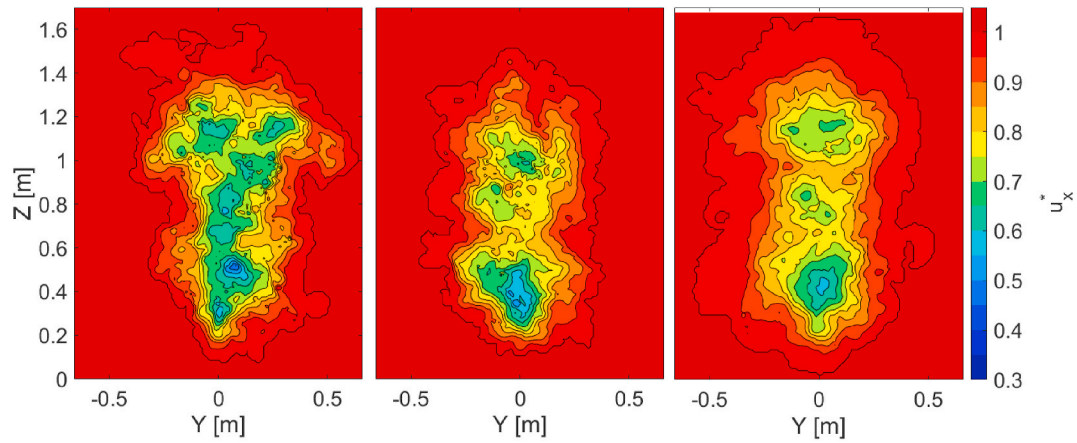
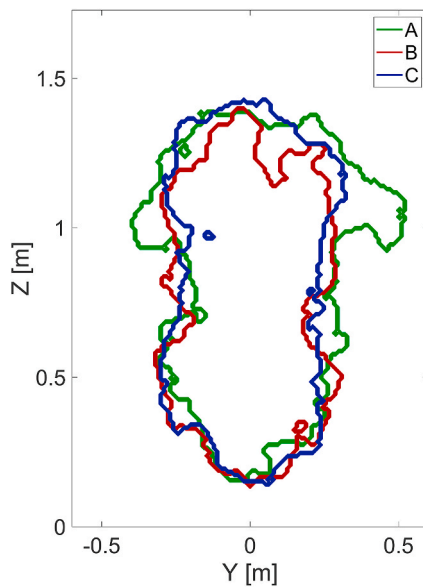**Fig. 6.** Ensemble-average velocity u_x^* at X = 0.5 m for cyclist A (left), B (middle) and C (right).

Fig. 7. Comparison of isolines of the ensemble-average velocity u_x^* equal to 0.9 among the three cyclists (X = 0.5 m).

region ($u_x^*<0.6$) vanishes after 2 m in the wake. From the top view in Fig. 9 one can appreciate the lateral spreading of the wake: at X = 6 m the velocity deficit exhibits approximately 1 m width. Comparatively the velocity distribution seems to spread less along the vertical direction. In

particular, the flow *downwash* past the cyclist (indicating the presence of a mild upwards force) moves the center of the wake towards the road. These observations are consistent with those reported by Spoelstra et al. (2019), where a similar wake evolution was found.

The potential drag reduction by drafting is analyzed here observing the spatial evolution of the velocity past a single athlete. The average streamwise velocity ($\overline{u_x}$)versus distance as well as the rate of lateral wake expansion versus distance in the near wake are presented in Fig. 10. The average streamwise velocity $\overline{u_x}$is defined as the average velocity in the wake of the cyclist, where the wake is determined by the contouring approach discussed in Spoelstra et al. (2020a). The lateral wake expansion is defined by the growth in the wake half-width y_w, which is evaluated as the distance from the maximum velocity to point where this velocity is half (Pope, 2000) in the XY-plane at Z = 0.8 m. In the near wake of the three cyclists the average streamwise velocity $\overline{u_x}$ decays with $\sim X^{-\frac{1}{3}}$ and their half-wake width y_w very slowly expands linearly with $\sim 0.04X$. These decay and expansion scales are represented by the gray dashed lines in Fig. 10. Furthermore, as a reference, the scaling laws for an axisymmetric wake as reported by Pope (2000) are indicated by the gray dash-dotted lines. According to Pope (2000), the velocity decays as $X^{-\frac{2}{3}}$ and the wake half-width, y_w, expands as $0.1\Delta X^{\frac{1}{3}}$.

Table 1 summarizes the ensemble-averaged drag area (C_dA_0), height, mass and projected frontal area measured for each cyclist participating in this experiment. As it can be observed, the projected frontal area is strongly dependent on the cyclist posture and as a result, it does not directly correlate with the athlete height or weight. The combination of frontal area and posture leads to a similar C_dA_0 value for cyclists A and C, whereas cyclist B exhibits a C_dA_0 about 10% smaller. The uncertainties of the drag area measurements are similar to those reported for previous RoF experiments, namely below 5% (Spoelstra et al., 2019).
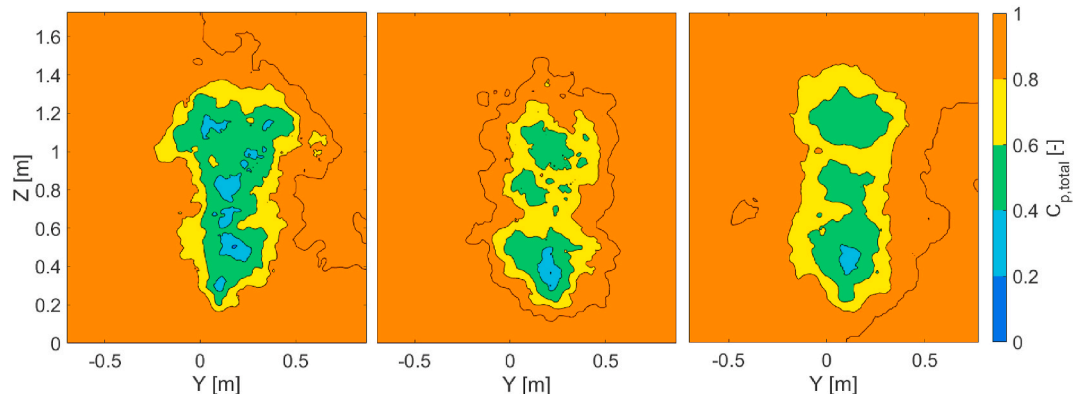

Fig. 8. Comparison of ensemble-averaged total pressure coefficient at X = 0.5 m, for cyclist A (left), B (middle) and C (right).
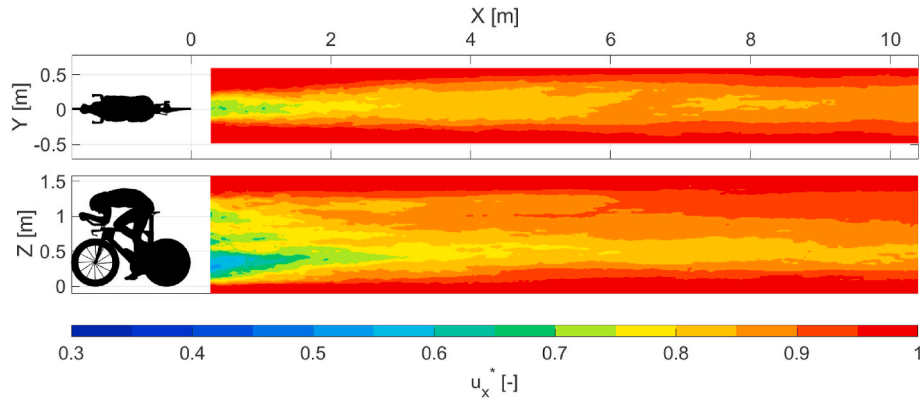
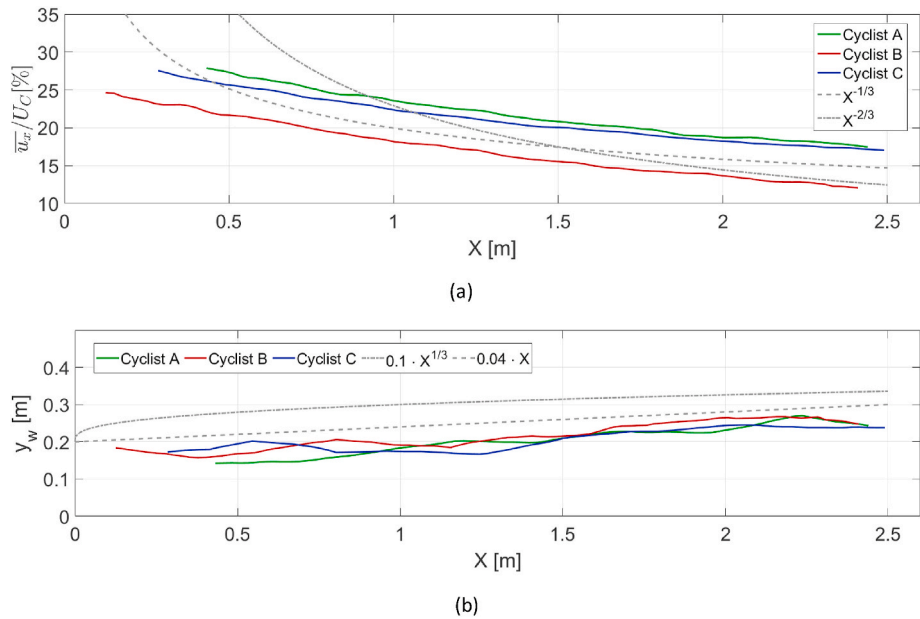**Fig. 9.** Top (Z = 0.8 m) and side view (Y = 0 m) of ensemble-averaged velocity past cyclist C.

Fig. 10. Average velocity decay and wake width. (a) The average streamwise velocity ($\overline{u_x}$) normalized by cyclist velocity (u_C) vs. distance in the wake for all three cyclists. (b) The average lateral wake expansion in the XY-plane at a height of Z = 0.8 m.

4.3. Tandem configuration

4.3.1. Flow field analysis

Three runs are chosen for the investigation of the flow fields in the tandem configurations; one where both longitudinal and lateral separation are small, one where longitudinal separation is large but lateral separation is still small, and finally one where both longitudinal and lateral separation are large. Those runs are labeled as I, II and III in Fig. 13, respectively. A summary of the separations for the three runs is presented in Table 3.

The instantaneous velocity fields of the three runs are compared in Fig. 11, with the first and second row corresponding to upstream and downstream of the trailing cyclist respectively. When comparing the inflow conditions of run I and II, it is observed that both trailing cyclists

Table 3
Longitudinal and lateral separations for drafting runs I, II, III.

Configuration	Longitudinal separation [m]	Lateral separation [m]
Run I (C–B)	0.35	0.01
Run II (B-A)	0.78	0.01
Run III (B-A)	0.85	0.18

are fully submerged in the wake of the leading cyclist. Since the inflow at run II is further downstream of the leading cyclist, it was expected that the velocity deficit created by the lead cyclist was already partly recovered to freestream conditions.

When the longitudinal separation was similar, but the lateral separation was increased (run III compared to run II), the velocity deficit created by the lead cyclist was similar; however, because the trailing cyclist in run III was not fully submerged in the wake of the leading cyclist, on average he encountered a higher inflow velocity. This is confirmed in Fig. 11.
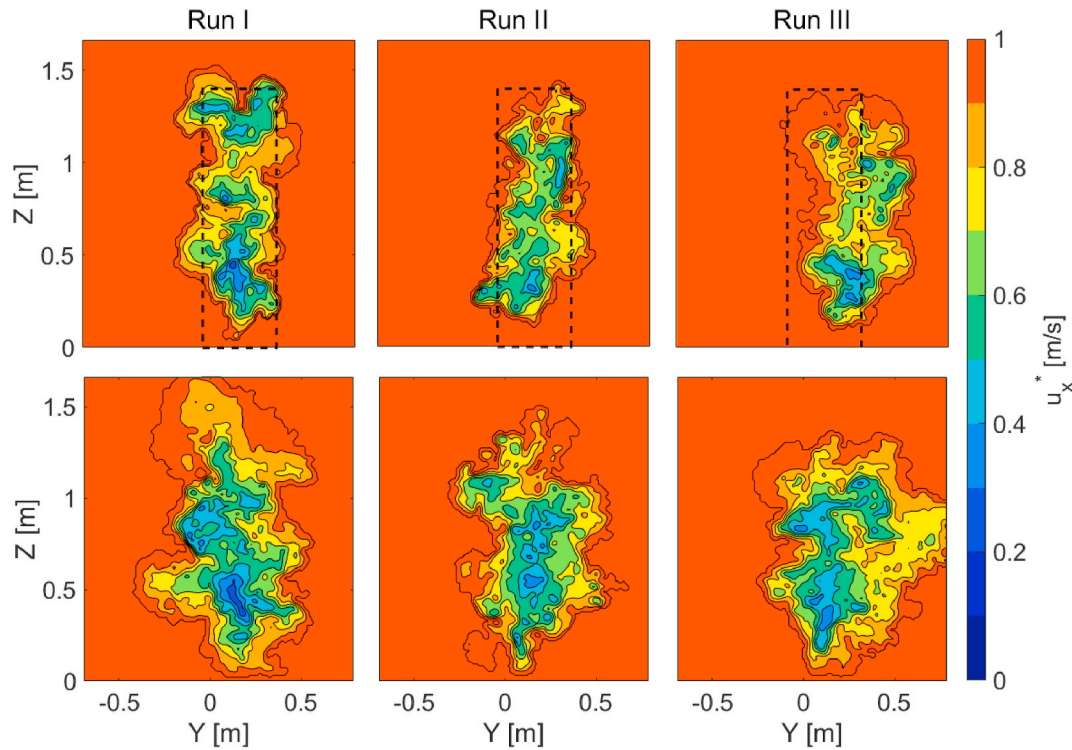
The instantaneous velocity field in the wake of the trailing cyclist (bottom row of Fig. 11) in all of the three cases shows a higher deficit than that of the ensemble-average velocity field in the wake of the isolated cyclist (Fig. 6). With larger longitudinal separation (run II and run III), the velocity deficit more closely resembles the single cyclist due to reduction of the influence of the velocity components in the leader's wake. In terms of wake width it is observed that for run I and II, with null lateral separation, there is little difference w.r.t. the individual cyclist. When however the lateral separation is increased (run III) the wake width significantly increases.

Under the assumption that the velocity deficit is small with respect to the cyclist velocity, using a simplified model, the drag of the cyclist is

Fig. 11. Instantaneous dimensionless filtered streamwise velocity (u_x^*) contours 0.1 m upstream of the trailing cyclist (top) and 0.5 m downstream of the trailing cyclist (bottom). The dashed rectangle indicates the location of the trailing cyclist relative to the wake of the leading cyclist.

given by the difference in total pressure between upstream and downstream of the cyclist, times the wake area (Jones, 1936). Hence, a decrease of total pressure upstream of the rider, or an increase of total pressure downstream of the rider would result in lower drag. Therefore, the instantaneous total pressure coefficient upstream and downstream of

the drafting cyclist is compared to the ensemble-average total pressure coefficient of the individual cyclists. In Fig. 12, the total pressure coefficient is plotted at the same locations as the velocity fields in Fig. 11. Similar observations can be made as were made for the velocity fields in Fig. 11 in terms of changes w.r.t. the individual cyclist.
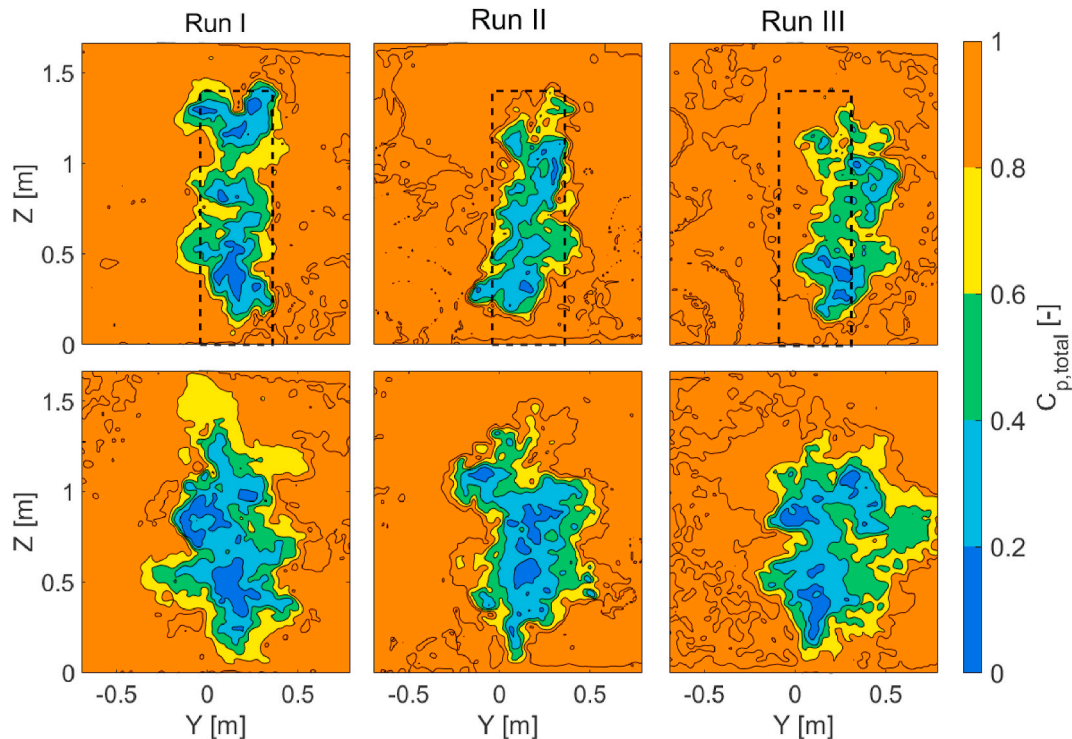
Fig. 12. Instantaneous total pressure coefficient ($C_{p,total}$) contours 0.1 m upstream of the trailing cyclist (top) and 0.5 m downstream of the trailing cyclist (bottom). The dashed rectangle indicates the location of the trailing cyclist relative to the wake of the leading cyclist.
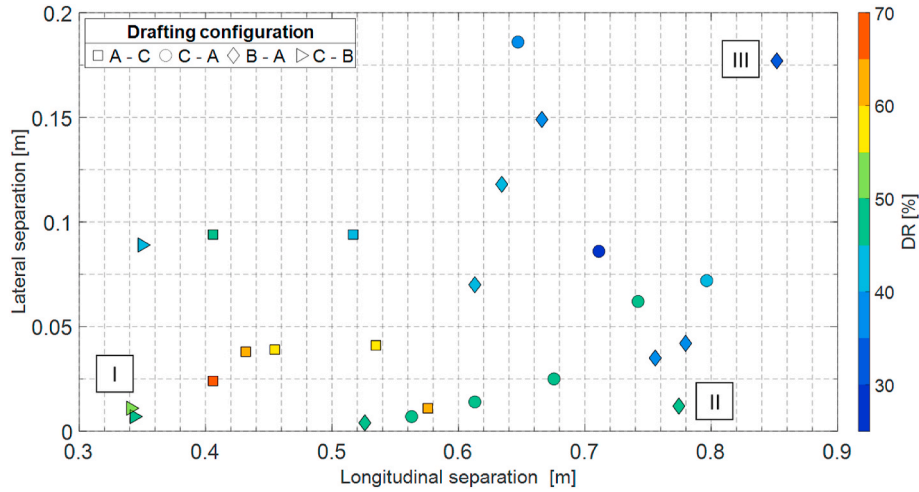
Fig. 13. Reduction in drag area for the drafting cyclist at different positions behind the lead cyclist. To obtain a better overview, all positions are plotted with a positive lateral separation and the lateral separation is exaggerated. In practice lateral separation occurred in both positive and negative direction.

Table 4 presents the differences in total pressure ($\Delta P_{tot} = (P_{tot,drafting}-P_{tot, individual})/P_{tot, individual}$). *Upstream* ΔP_{tot} is defined as the difference in instantaneous total pressure in front of the drafting cyclist and the ensemble-average total pressure in front of that same cyclist riding alone. *Downstream* ΔP_{tot} is defined as the difference in instantaneous total pressure drop behind the drafting cyclist and the sum of the ensemble-averaged total pressure drop behind both individual cyclists participating in the drafting configuration; an example could be a drafting configuration where the total pressure coefficient behind each rider drops by 25% when riding individually, and the total pressure drop behind the peloton is 40%, then *downstream* $\Delta P_{tot} = 40\% - (2 \times 25\%) = -10\%$.

The results presented in Table 4 show that upstream of the drafting cyclist there is an average decrease of 45%, 35%, and 23% in total pressure for runs I, II and III, respectively. Following the methodology described in section 2, the drag reductions for the drafting cyclists in the three cases are found to be equal to 52%, 46% and 31%. This shows that the average drop in total pressure in front of the drafting cyclist is still underestimating the observed drag reductions slightly and thus part of the drag reduction should be found in the *Downstream* ΔP_{tot}. For run I the downstream ΔP_{tot} is -4%, for run II and III this is -9% and -10%, respectively. This means higher total pressures in the wake of the drafting cyclist as compared to the sum of both individuals, resulting in a further reduction in the drag of the trailing cyclist.

According to these findings, the sum of the difference in total pressure upstream and downstream of the drafting cyclist is close to the total drag reduction. Similar to findings in literature, all three cases show that the change in inflow conditions is the main cause of the drag reduction; however, with a difference up to 10%, the change in total pressure in the wake cannot be neglected. Additionally, it is observed that the bigger the longitudinal gap becomes, the bigger the effect on total pressure in the wake becomes.

Table 4
Drag reduction measured per configuration and the changes in spatial-average $C_{p,tot}$ upstream and downstream of the cyclist when drafting as compared to riding alone.

Configuration	Upstream Δ P_{tot} [%]	Downstream Δ P_{tot} [%]	Sum P_{tot} reduction [%]	Drag reduction [%]
Run I (C–B)	−45	−4	49	52
Run II (B-A)	−35	−9	44	46
Run III (B-A)	−23	−10	33	31

4.3.2. Drag analysis

The results of the drag reduction from the RoF measurements as a function of the longitudinal and lateral spacing between the riders are summarized in Fig. 13. To obtain a better overview, all positions are plotted with a positive lateral separation. In practice lateral separation occurred in both positive and negative direction. Drag reductions between 27% and 67% are observed with a general inverse relationship between drag reduction and drafting distance, with high reductions where both longitudinal and lateral distances are low and low drag reductions where the lateral offset is higher. It is observed that the effect of lateral separation is much stronger than longitudinal separation, which is in agreement with Barry et al. (2014) and Zdravkovich (1996). The drag reduction of cyclist C in the configuration A–C is significantly higher than that found in the other configurations in the current study as well as those found by Barry et al. (2014), up to 67%. However a similar trend is observed: the drag reduction shows higher dependency on lateral displacements than on the longitudinal one. The higher drag reduction in this configuration is associated with the higher frontal area of A; as a consequence, the cyclist drafting behind rider A experiences the minimum total pressure inflow.

4.4. Modelling drag reduction

A semi-empirical model is attempted here for the use of predicting drag reduction under similar drafting conditions as the ones in the current experiment. In section 4.3.1 it was found that the drag reduction under drafting is proportional to the drop in total pressure, or kinetic energy (u^2), at the location of the drafting cyclist. In order to find a mathematical expression for the drag reduction, we need to find an expression for the spatial evolution of the velocity past a single athlete. The average streamwise velocity ($\overline{u_x}$) versus distance as well as the rate of lateral wake expansion versus distance in the near wake of a single athlete were presented in Fig. 10 in section 4.2. It is assumed that the wake of a cyclist can be approximated as an axisymmetric wake flow behind a bluff body. Pope (2000) describes the following similarity relations for such a wake:

$$y_w(x) \sim x^{\frac{1}{3}}, \frac{u_s(x)}{U_\infty} \sim x^{-\frac{2}{3}}, f(\xi) = e^{-B\xi^2}, \xi = \frac{y}{y_w(x)} \tag{4}$$

where y_w is the wake half-width, u_s is defined as the centerline velocity deficit, U_∞ is the upstream velocity, ξ is the scaled cross-stream variable, $f(\xi)$ is the self-similar velocity defect and B is a non-dimensional constant. In section 4.2 we described that the velocity deficit in the wake of a cyclist approximately decays with $x^{-1/3}$, whereas the wake width

expands linearly with *x*. Taking these findings into consideration, a mathematical expression for the drag reduction is proposed as follows:

$$DR(X, Y) = A \cdot X^{-1/3} \cdot e^{-B \cdot \left(\frac{Y}{X} \right)^2} \tag{5}$$

where *A* and *B* are parameters to be determined from the input of experimental or computational data. The parameters *X* and *Y* in equation (5) are the longitudinal and lateral separation, respectively. The separation, in this work, is taken as the distance between the trailing edge of the rear wheel of the leading cyclist to the leading edge of the front wheel of the trailing one. The largest cross section and thus largest contributor to the drag force, however, is given by the athlete's body; at zero separation (no gap between the wheels), the distance between the bodies of the riders (from the lower back lead rider to head of trailing rider) is of the order of two characteristic length scales. The characteristic length scale for a cyclist wake *c* is considered to be the shoulder width, approximately *c* = 0.4 m.

4.4.1. Model input data and uncertainty

In order to estimate the model parameters described in equation (5), data needs to be fitted to the model. Since the data set obtained by the Ring of Fire, as described in section 4.3.2, only comprises 25 data points (50 when symmetry about the *XZ*-plane is assumed), the drag measurements from Barry et al. (2014) are added to the data set, increasing the total amount of data points to 100. Barry et al. (2014) carried out measurements in the wind tunnel with two full-scale models on time-trial bikes at a test velocity of 18 m/s. The drafting locations tested by Barry et al. (2014) are ranging from 0.1 to 0.7 m and 0–0.275 m in longitudinal and lateral direction, respectively. The combined data set was fitted to the model by the non-linear least-squares method and in order to minimize the influence of outliers, the method of Bi-square weights was applied (Yu and Yao, 2017). The parameters *A* and *B* are estimated with 95% confidence intervals, yielding $A = 35.3 \pm 2$ m$^{1/3}$ and $B = 1.04 \pm 0.3$ respectively. The predicted DR obtained from the model has a RMSE of 9.9 and R-square of 0.28 and is plotted in Fig. 14 alongside the data points used for fitting. As the range of the combined data set is limited to $0.1m \leq X \leq 1m$ and $-0.3m \leq Y \leq 0.3m$, the range of validity of this model with the estimated parameters *A* and *B* is limited to this region. Furthermore, it should be noted that this model is only valid for two cyclists in time-trial posture, as adding more riders or changing posture will influence the drag reduction of the second rider (Blocken et al., 2013, 2018).

Fig. 15 compares the DR reported in literature to the DR found by our model. On the left the change in DR w.r.t. change in longitudinal distance at 0 lateral offset is presented, in the middle and on the right the change in DR with lateral distance at 0.3 and 0.7 m longitudinal offset, respectively, is shown. Close to the leading cyclist, (longitudinal <0.3 m and lateral = 0 m), the model yields some overestimated drag reduction compared to literature, which indicates that more data points might be needed close to the leading cyclist in order to get a better fit of the model. When the trailing cyclist is laterally offset, the predictions of the proposed model shows a similar rate of decline in DR as compared to what was found by Zdravkovich (1996); however the predicted DR by our model is higher, which may be due to the difference in experimental conditions.

5. Conclusions

Ring of Fire experiments have been carried out to investigate the aerodynamics of cyclists riding at short distance from each other (drafting). The drag force is inferred from a momentum conservation approach that is adapted from Spoelstra et al. (2019) where the aerodynamic drag from individual athletes was determined. The flow field visualizations show that the amount of drag reduction of the trailing rider should be mainly ascribed to the inflow conditions featuring a pronounced momentum deficit. Within the measured range of longitudinal separation, the drag reduction for the drafting cyclist ranges from 27% to 67%. The aerodynamic advantage, however, decreases as the lateral and longitudinal separation between riders is increased, where the lateral distance is found to produce a more rapid effect. A mathematical expression is proposed that describes a model introduced to predict the drag reduction under drafting conditions. Input from current experiments as well as from literature data returns a realistic prediction of the drag reduction in the near wake with an overestimation of the drag reduction at longitudinal distance between 0.1 m and 0.3 m.

Besides the above results, the RoF demonstrates its potential to investigate cycling aerodynamics and simultaneously monitor the drafting skill level of cyclists, which is currently not practiced with the
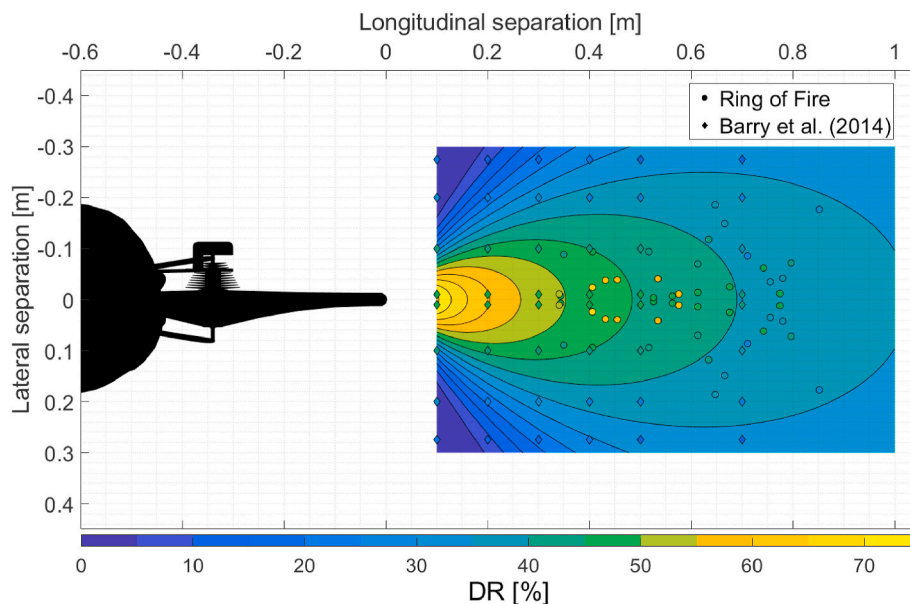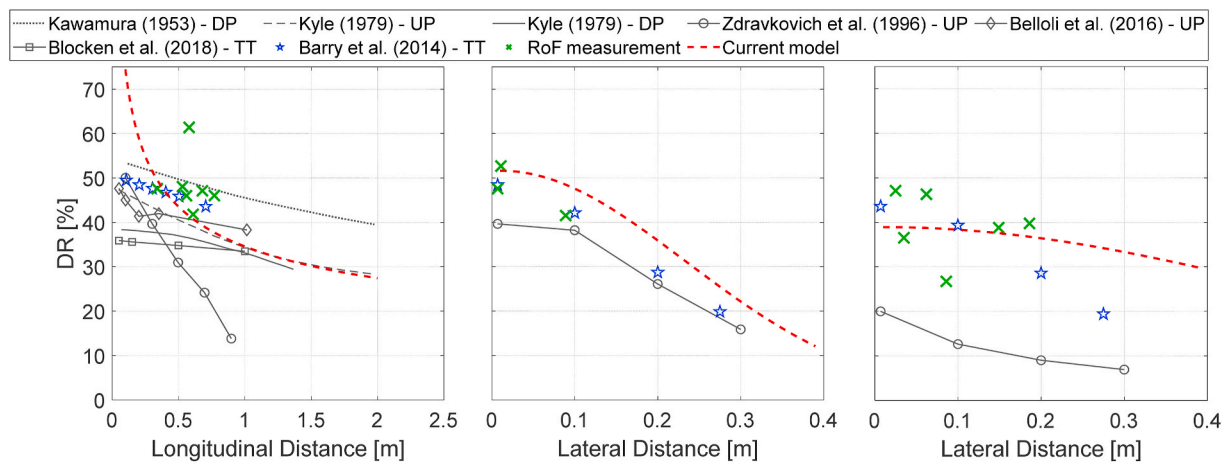

Fig. 14. Drag reduction according to the mathematical model described by equation (5) (color contours), based on data input from the current experiments (color-coded circles) and from Barry et al. (2014) (color-coded diamonds). (For interpretation of the references to color in this figure legend, the reader is referred to the Web version of this article.)

Fig. 15. Trailing cyclist drag reduction by longitudinal and lateral offset reported in literature and from the mathematical model described in this work. Left: effect of longitudinal distance taken at zero lateral offset. Middle: effect of lateral distance taken at 0.3 m longitudinal separation. Right: effect of lateral distance taken at 0.7 m longitudinal separation.

current state-of-the-art measurement techniques for cycling aerodynamics.

CRediT authorship contribution statement

Alexander Spoelstra: Conceptualization, Investigation, Methodology, Visualization, Writing – original draft. **Andrea Sciacchitano:** Conceptualization, Investigation, Methodology, Supervision, Writing – review & editing. **Fulvio Scarano:** Supervision, Writing – review & editing. **Nikhil Mahalingesh:** Investigation, Writing – review & editing.

Declaration of competing interest

The authors declare that they have no known competing financial interests or personal relationships that could have appeared to influence the work reported in this paper.

Acknowledgments

References

Barry, N., Burton, D., Sheridan, J., Thompson, M., Brown, N.A.T., 2015. Aerodynamic drag interactions between cyclists in a team pursuit. Sports Eng. 18 (2), 93–103. https://doi.org/10.1007/s12283-015-0172-8.

Barry, N., Burton, D., Sheridan, J., Thompson, M., Brown, N.A.T., 2016. Flow field interactions between two tandem cyclists. Exp. Fluid 57 (12). https://doi.org/10.1007/s00348-016-2273-y.

Barry, N., Sheridan, J., Burton, D., Brown, N.A.T., 2014. The effect of spatial position on the aerodynamic interactions between cyclists. In: Paper Presented at the Procedia Engineering.

Blocken, B., Defraeye, T., Koninckx, E., Carmeliet, J., Hespel, P., 2013. CFD simulations of the aerodynamic drag of two drafting cyclists. Comput. Fluids 71, 435–445. https://doi.org/10.1016/j.compfluid.2012.11.012.

Blocken, B., Toparlar, Y., van Druenen, T., Andrianne, T., 2018. Aerodynamic drag in cycling team time trials. J. Wind Eng. Ind. Aerod. 182, 128–145. https://doi.org/10.1016/j.jweia.2018.09.015.

Broker, J.P., Kyle, C.R., Burke, E.R., 1999. Racing cyclist power requirements in the 4000-m individual and team pursuits. Med. Sci. Sports Exerc. 31 (11), 1677–1685. https://doi.org/10.1097/00005768-199911000-00026.

Crouch, T.N., Burton, D., Brown, N.A.T., Thompson, M.C., Sheridan, J., 2014. Flow topology in the wake of a cyclist and its effect on aerodynamic drag. J. Fluid Mech. 748, 5–35. https://doi.org/10.1017/jfm.2013.678.

Defraeye, T., Blocken, B., Koninckx, E., Hespel, P., Verboven, P., Nicolai, B., Carmeliet, J., 2014. Cyclist drag in team pursuit: influence of cyclist sequence, stature, and arm spacing. J. Biomech. Eng. 136 (1) https://doi.org/10.1115/1.4025792.

Edwards, A.G., Byrnes, W.C., 2007. Aerodynamic characteristics as determinants of the drafting effect in cycling. Med. Sci. Sports Exerc. 39 (1), 170–176. https://doi.org/10.1249/01.mss.0000239400.85955.12.

Fitton, B., Caddy, O., Symons, D., 2018. The impact of relative athlete characteristics on the drag reductions caused by drafting when cycling in a velodrome. Proc. Inst. Mech. Eng. P J. Sports Eng. Technol. 232 (1), 39–49. https://doi.org/10.1177/1754337117692280.

Íñiguez-De-La Torre, A., Íñiguez, J., 2009. Aerodynamics of a cycling team in a time trial: does the cyclist at the front benefit? Eur. J. Phys. 30 (6), 1365–1369. https://doi.org/10.1088/0143-0807/30/6/014.

Jones, B., 1936. Measurement of Profile Drag by the Pitot-Traverse Method. ARC R&M, p. 1688.

Kawamura, T.M., 1953. Wind Drag of Bicycles. Tokyo University. Report No.1.

Kyle, C.R., 1979. Reduction of wind resistance and power output of racing cyclists and runners travelling in groups. Ergonomics 22 (4), 387–397. https://doi.org/10.1080/00140137908924623.

Olds, T., 1998. The mathematics of breaking away and chasing in cycling. Eur. J. Appl. Physiol. Occup. Physiol. 77 (6), 492–497. https://doi.org/10.1007/s004210050365.

Pope, S.B., 2000. Turbulent Flows. Cambridge University Press, Cambridge.

Raffel, M., Willert, C.E., Scarano, F., Kähler, C.J., Wereley, S.T., Kompenhans, J., 2018. Particle Image Velocimetry: a Practical Guide. Springer.

Scarano, F., Ghaemi, S., Caridi, G.C.A., Bosbach, J., Dierksheide, U., Sciacchitano, A., 2015. On the use of helium-filled soap bubbles for large-scale tomographic PIV in wind tunnel experiments. Exp. Fluid 56 (2), 42. https://doi.org/10.1007/s00348-015-1909-7.

Spoelstra, A., de Martino Norante, L., Terra, W., Sciacchitano, A., Scarano, F., 2019. On-site cycling drag analysis with the Ring of Fire. Exp. Fluid 60 (6), 90. https://doi.org/10.1007/s00348-019-2737-y.

Spoelstra, A., Hirsch, M., Sciacchitano, A., Scarano, F., 2020a. Uncertainty Assessment of the Ring of Fire Concept for On-Site Aerodynamic Drag Evaluation. Measurement Science and Technology.

Spoelstra, A., Mahalingesh, N., Sciacchitano, A., 2020b. Drafting effect in cycling: on-site aerodynamic investigation by the 'ring of Fire, 2020 Proceedings 49 (113). , 49(113).

Terra, W., Sciacchitano, A., Scarano, F., 2017. Aerodynamic drag of a transiting sphere by large-scale tomographic-PIV. Exp. Fluid 58 (7), 83. https://doi.org/10.1007/s00348-017-2331-0.

van Oudheusden, B.W., 2013. PIV-based pressure measurement. Meas. Sci. Technol. 24 (3), 032001 https://doi.org/10.1088/0957-0233/24/3/032001.

Yu, C., Yao, W., 2017. Robust linear regression: a review and comparison. Commun. Stat. Simulat. Comput. 46 (8), 6261–6282. https://doi.org/10.1080/03610918.2016.1202271.

Zdravkovich, M.M., 1996. Effect of cyclist's posture and vicinity of another cyclist on aerodynamic drag. In: Haake, S. (Ed.), The Engineering of Sport. Balkema, Rotterdam.